

Ages of Elliptical Galaxies: Single versus Multi Population Interpretation

T.P. Idiart¹, J. Silk², José A. de Freitas Pacheco³

¹ Instituto de Astronomia, Geofísica e Ciências Atmosféricas, Rua do Matão 1226, S. Paulo, Brasil

² Astrophysics, Denys Wilkinson Building, Keble Road, Oxford OX1 3RH, UK

³ Observatoire de la Côte d’Azur, B.P.4229, F-06304 Nice Cedex 4, France
 emails: thais@astro.iag.usp.br; silk@astro.ox.ac.uk; pacheco@obs-nice.fr

august/2007

ABSTRACT

New calibrations of spectrophotometric indices of elliptical galaxies as functions of spectrophotometric indices are presented, permitting estimates of mean stellar population ages and metallicities. These calibrations are based on evolutionary models including a two-phase interstellar medium, infall and a galactic wind. Free parameters were fixed by requiring that models reproduce the mean trend of data in the color-magnitude diagram as well as in the plane of indices $H\beta$ - Mg_2 and Mg_2 - $\langle Fe \rangle$. To improve the location of faint ellipticals ($M_B > -20$) in the $H\beta$ - Mg_2 diagram, down-sizing was introduced. An application of our calibrations to a sample of ellipticals and a comparison with results derived from single stellar population models is given. Our models indicate that mean population ages span an interval of 7-12 Gyr and are correlated with metallicities, which range from \sim half up to three times solar.

Key words: elliptical galaxies, population synthesis, metallicity and age calibrations

1 INTRODUCTION

The formation of galaxies is certainly one of the most challenging open problems in cosmology, since theory must account for the evolution and integrated galaxy properties (Silk 2004). Among the different morphological types, elliptical (E) galaxies are the simplest ones, with mass indicators like the central velocity dispersion presenting robust correlations with different spectrophotometric properties (see de Freitas Pacheco, Michard & Mohayaee 2003 for a review). From a theoretical point of view, different formation scenarios have been proposed: one is monolithic collapse, in which the gaseous material is assembled either in the form of a unique cloud (Larson 1974a) or by interaction and merging of a hierarchy of many primeval lumps of matter, not including pre-existing stars, into a proto-galaxy (Peebles 2002; Matteucci 2003). The alternative picture, that of hierarchical merging, considers that galaxies form from successive non-dissipative mergers of small-scale halos over a wide redshift range (White & Rees 1978; Toomre 1977; Kauffmann 1996; Baugh et al. 1996, 1998). Thus, a fundamental aspect is whether any of the observable properties of Es contains an imprint of their previous

formation history which, in essence, is related to the stellar population formation history. Therefore, the key questions are when the bulk of stars was formed and if ellipticals evolved passively or were modified, and to what extent, by interactions with the environment.

In this context, the age distribution of stellar populations in E galaxies is essential to understand their origin and evolution. Absorption line indices combined with colors are powerful tools to derive ages and metallicities of the stellar populations constituting early type galaxies. However, the interpretation of these integrated spectral characteristics necessarily requires the use of models. In the past, this exercise has been accomplished by different authors using either single stellar population models (SSP) or evolutionary models (EVM).

SSP models are straightforward applications of the theory of stellar evolution. Given an initial mass function (IMF) and chemical composition, the evolution of such a population and its corresponding spectral characteristics are completely defined. Properties of E galaxies derived from observed spectral indices and SSP models were obtained by Worthey (1994), Trager et al.(2000), Thomas, Maraston & Bender (2003) and, more recently

by Howell (2005), among others. Most of these studies have concluded that E galaxies present a small spread in metallicity but span a wide range of ages.

Elliptical galaxies are certainly not single population systems and the reason generally invoked to interpret data by using SSP models, besides simplicity, is that the bulk of stars in Es formed on a short time-scale and, consequently all stars should have similar ages. Even if the age range of the population mix constituting the galaxy would be quite narrow, the build-up of chemical elements requires successive stellar generations, which are necessarily described by a metallicity distribution. Analyses of mid-ultraviolet indices by Lotz, Ferguson & Bohlin (2000) clearly demonstrate that single-age and single-metallicity populations are able to explain globular cluster data (true single population systems) but not Es. Analytical models are, in general, of the “one-zone” type including (or not) mass loss from galactic winds or infall of matter from the intergalactic medium. Star formation begins when a critical gas density is attained and the evolution of the population mix is calculated by summing the properties of SSP models, representative of successive stellar generations. Their formation rate is controlled by the amount of residual gas available for star formation, whereas their chemical composition results from the progressive enrichment in “metals” of the interstellar medium (ISM) by matter ejected from stars, notably supernovae. Examples of evolutionary models can be found in Matteucci & Tornambè (1987), Bressan, Chiosi & Tantalò (1996), Vazdekis et al. (1996), Kodama & Arimoto (1997), Idiart, Michard & de Freitas Pacheco (2003, hereafter IMP03). In general, these models lead to mean metallicities and $[Mg/Fe]$ ratios comparable to those derived from SSP models, but significant disagreements remain on age determinations of the bulk stellar population.

In the present work, new calibrations of spectrophotometric indices permitting estimates of mean ages and metallicities of the stellar population mix constituting early-type galaxies are reported. These calibrations are based on evolutionary models in which the free parameters were adjusted in order to adequately reproduce not only the color-magnitude diagram (CMD) but also the observed strength of indices like $H\beta$, Mg_2 and $\langle Fe \rangle$. In spite of adopting the classical “one-zone” approximation, the present model simulates the existence of a two-phase ISM in which stars are formed only in cold gas regions, allowing also a gradual assembly of the galaxy as well as the presence of a galactic wind. The anticorrelation between the indices $H\beta$ and Mg_2 can be explained if we make appeal to the down-sizing effect (Cowie et al. 1996). Thus, in our model sequence, the less massive galaxies are assembled later ($z \sim 0.8$) than the more massive ones ($z \sim 3-4$). We have also assumed that dust is mixed with the residual gas producing a small internal reddening, which improves the fit of the aforementioned diagrams. This paper is organized as follows: in Section 2 the main features of the model are described; in Section 3 the results for a grid of fiducial models are presented as well as the resulting calibra-

tions for mean ages and metallicities; finally, in Section 4 the main conclusions are given.

2 THE MODEL

2.1 The mass balance equations

The model is based on the “one-zone” approximation and thus it cannot predict spatial variations. However, when performing the mass balance, we have assumed that the gas is either in a hot or in a cold phase, where the former is a consequence of mass ejection by evolved stars and hot gas “cavities” produced by supernova explosions. The presence of hot gas in bright ellipticals is well established by X-ray observations, which indicate the existence of diffuse thermal emission in these objects and, observations indicate also that cold molecular clouds and not the hot gas phase are the sites of star formation. Two-phase models have been considered in the past and, among others, we mention the work by Ferrini & Poggianti (1993) and that by Fujita, Fukumoto & Okoshi (1996), who have initially adopted an “one-zone” model and, in a subsequent investigation, considered a spherical galaxy with a given mass distribution to study local properties (Fujita, Fukumoto & Okoshi 1997). Here, a more simplified version of these approaches is considered. In order to establish the mass balance equations, we consider that, as a consequence of the stellar evolution, the gas returns to the medium, contributing to the hot phase. Supernovae are additional sources of hot gas since they inject mechanical energy into the interstellar medium through blast waves produced by the explosion. The onset of a galactic wind removes hot gas from the system and radiative cooling followed by recombination processes transforms part of the hot gas into the cold phase.

Define the gas fraction $f_g(t)$ as the ratio between the total gas mass present in the galaxy at instant t and M_0 , a quantity representing the total mass acquired by the galaxy by “infall” processes (“infall” here means continuous accretion or sudden variations of mass by merging events). If $f_h(t)$ and $f_c(t)$ are respectively the gas fractions in the hot and in the cold phases, define $x_h(t) = f_h(t)/f_g(t)$ and $x_c(t) = f_c(t)/f_g(t)$ such that $x_h(t) + x_c(t) = 1$. Under these conditions, two equations are required to describe the evolution of the total gas fraction $f_g(t)$ and, for instance, the fraction $x_h(t)$ in the hot phase, since $x_c(t) = 1 - x_h(t)$.

The equation governing the total gas fraction $f_g(t)$ evolution can be written as

$$\frac{df_g(t)}{dt} = -k(1 - x_h(t))f_g(t) + \frac{df_{ej}(t)}{dt} - \frac{x_h(t)f_g(t)}{\tau_w} + \dot{R}_{in} \quad (1)$$

The first term on the right represents the amount of cold gas which is transformed into stars. The star formation rate normalized with respect to M_0 , $R_*(t) = kx_c(t)f_g(t)$, was assumed to be proportional to the available amount of cold gas, with an efficiency k given in Gyr^{-1} . The second term represents the gas returned to the ISM at a rate

$$\frac{df_{ej}(t)}{dt} = k \int_{m(t)}^{m_s} (m - m_r) \zeta(m) R_*(t - \tau_m) dm \quad (2)$$

The upper limit of the integral was taken equal to $80M_\odot$ and the lower limit corresponds to the stellar mass whose lifetime is equal to t . In the integrand, m_r is the mass of the remnant, which depends on the progenitor mass, $\zeta(m) = A/m^\gamma$ is the initial mass function (IMF) and the star formation rate is to be taken at the retarded time ($t - \tau_m$), where τ_m is lifetime of a star of mass m . The adoption of a power-law at low masses for the IMF is a simplifying assumption that has no bearing on our results, which depend only on the slope at the massive end, which we indeed will vary as a model parameter. The third term represents the mass loss by the galactic wind, whose rate was assumed to be proportional to the amount of hot gas. Finally, the last term gives the rate at which the galaxy accretes mass, here assumed to be of the form $\dot{R}_{in} \propto e^{-t/t_{in}}$.

The second equation, which describes the evolution of the fraction $x_c(t)$ of hot gas is

$$\begin{aligned} \frac{dx_h(t)}{dt} = & -x_h(t) \frac{d(f_g(t))}{dt} + \frac{m_H}{M_0} \frac{1}{f_g(t)} \sum Q_i \nu_i \\ & + \frac{1}{f_g(t)} \frac{df_{ej}}{dt} - \frac{\alpha(T)M_0}{m_H V_g} x_h^2(t) f_g(t) - \frac{x_h(t)}{\tau_w} \end{aligned} \quad (3)$$

In this equation, the first term on the right, since $x_h(t)$ is defined with respect to the total gas fraction, takes into account the time variation of the “background”. The second term represents the production of hot gas by supernovae and the sum is performed over both types Ia and II; Q is the mean number of atoms converted into the hot phase per explosion. This number corresponds to the amount of interstellar gas swept by the blast wave when forming the “hot cavity”. Using the Sedov theory, $Q = 1.35E/(m_H V_s^2)$, where E is the energy of the explosion and V_s is the shock velocity. As in Fujita, Fukumoto & Okoshi (1997), we assume that the hot gas cavity ends its evolution when the shock velocity is comparable to the stellar velocity dispersion. The frequency ν_{II} of type II supernovae was estimated by considering that only stars in the range $9 - 45M_\odot$ explode, whereas the frequency ν_{Ia} of type Ia supernovae was calculated as in Idiart, de Freitas Pacheco & Costa (1996). The third term corresponds to the contribution of the returned gas (see above) and the fourth term gives the rate at which the hot gas, after cooling, recombines into neutral and cold gas. In this term, $\alpha(T)$ is the effective recombination coefficient and V_g is the volume occupied by the gas, identified with the volume of the galaxy. We have assumed a spherical galaxy whose radius is fixed at any time by the radius-mass relation given by Gibson (1997). Finally, the last term gives the rate at which the hot gas is removed by the galactic wind.

Besides the gas evolution, the chemical enrichment of the galaxy is also followed. The chemical evolution is described by the usual equations but includes the contribution of the “infall” term, which dilutes the abundances of heavy elements and the contribution of the wind, which removes enriched gas and modifies the chemical composition of the nearby primordial inter-

galactic medium. Yields for massive stars were taken from Nomoto et al. (1997a) and those from type Ia supernova were taken from model W7 by Nomoto et al. (1997b).

2.2 Spectrophotometric indices

Integrated luminosities for SSP models for different photometric filters were recalculated by taking into account variations in the exponent of the IMF, in order to obtain self-consistent results. In fact, as in our previous study (IMP03), small variations of the IMF exponent γ were required in order to increase the magnesium yield. The color-magnitude diagram (CMD) of ellipticals is conventionally interpreted as a mass-metallicity sequence. Larson (1974b) suggested that such a sequence could be explained by a galactic wind able to gradually halt the star formation process as the galaxy mass increases. However, a longer duration of the star formation activity also increases the contribution of type Ia supernovae to the enrichment of the ISM, leading to an enhancement of iron relative to α -elements, contrary to the observed trend (Matteucci & Tornambè 1987; Worthey 1998). This problem can be partially surmounted if one assumes that massive E galaxies have flatter IMFs (Worthey 1998; Tantalo et al. 1998). In fact, in spite of all uncertainties involving theoretical yields from type II supernovae, there is agreement between different calculations that the Mg/Fe ratio increases considerably with decreasing metallicity of progenitors. Moreover, such a ratio varies strongly according to the progenitor mass: the ejecta of type II supernova progenitors with masses around 10-13 M_\odot have an abundance ratio $[Mg/Fe] \sim -1.9$. This ratio is near solar for progenitors of $\sim 20 M_\odot$ and suprasolar ($[Mg/Fe] \sim +1.4$) for masses around 70 M_\odot (Thielemann et al. 1996). Clearly, a flatter IMF for increasing galaxian masses alleviates not only the iron index problem but also permits, in combination with a varying star formation efficiency, a better representation of the CMD.

Evolutionary tracks required for our computations of photometric indices were taken from Girardi et al. (2000) and Salasnich et al. (2000), who have computed stellar models with non-solar abundances. The conversion of the iron abundance to the metallicity Z was performed by using the relation by Salaris et al. (1993), parameterized as a function of the excess of α -elements with respect to solar values and corrections suggested by Kim et al. (2002) for high metallicities. As first pointed out by Borges et al. (1995), population synthesis based on empirical stellar libraries inevitably reflects the chemical history of our Galaxy. Thus, functions describing the variation of indices in terms of atmospheric parameters like temperature, gravity and $[Fe/H]$ must also include the dependence on the $[\alpha/Fe]$ ratio. We have also revised our previous index calibrations (Idiart & de Freitas Pacheco 1995; Borges et al. 1995), includ-

ing additional stellar data to our library in order to have a better representation of solar and non-solar objects¹.

2.3 The computation procedure

In IMP03, models were tailored to reproduce the CMD of Es in Coma and Virgo, since this relation is tight for cluster ellipticals, whereas the scatter increases for Es in the nearby field and in small groups (Schweizer & Seitzer 1992). Here a different approach was adopted. Since we have searched for models able to reproduce simultaneously different spectrophotometric indices, a sample of E-galaxies was prepared, including objects with available total magnitudes, which are more representative of colors computed by modelers (see, for instance, a discussion in Scodreggio 2001 and Kaviraj et al. 2005) as well as other spectrophotometric data ($H\beta$, Mg_2 and $\langle Fe \rangle$ indices), required to fix the parameters of our models.

The system of equations to be solved has three main free parameters: the star formation efficiency k , the “in-fall” time-scale and the exponent of the IMF. The wind time-scale τ_w is not a real independent parameter as we shall see below. Initially, a grid of models was computed under the assumption that the star formation activity begun at the same time for galaxies of all masses. If this hypothesis implies that galaxies have the same age, it does not imply that their stellar populations have the same mean age, because the star formation rate is not necessarily the same for galaxies of different masses. Each model in the grid is characterized by the total mass M_0 acquired by infall. Once this parameter is fixed, for a given value of t_{in} , the initial accretion rate is fixed. In a second step, we adopt a value for the star formation efficiency k . Miranda (1992) derived from hydrodynamic models for the spherical collapse, including a galactic wind, a relation between the fraction of gas lost f_w by the galaxy and parameters characterizing the gravitational potential well and the star formation efficiency, as an indicator of the supernova heating. His results can be quite well fitted by the expression

$$\log f_w = 2.150 - 0.294 \log M_0 + 0.222 \log (kT_{age}) \quad (4)$$

Adopting this relation, the value of the wind parameter τ_w is immediately fixed. The numerical solution was performed without using the “instantaneous recycling approximation”, leading to the metallicity distribution function required to compute the integrated spectrophotometric properties as in Idiart, de Freitas Pacheco & Costa (1996). For different values of M_0 , a sequence of models was computed in which the aforementioned free parameters were varied in order to reproduce data on the diagrams $(U-V) - M_B$, $H\beta - Mg_2$ and $Mg_2 - \langle Fe \rangle$.

If, as in IMP03, the trend of data in the CMD can be well reproduced, this approach leads to faint galaxies with $H\beta$ indices systematically smaller than observations. A possible interpretation of the observed inverse

correlation between the indices $H\beta$ and Mg_2 was already given in the early 90s either by Sadler (1992) or by Faber, Worthey & Gonzalez (1992), who concluded that the stellar populations of the brightest Es are older than less luminous objects. This is consistent with the work by Cowie et al (1996), who, based on analysis of the luminosity function in the K band of deep fields, concluded that “the mass of star forming galaxies decreases with redshift”, immortalized as the down-sizing effect (see also Juneau et al. 2005). More recent data derived from deep surveys ($z \sim 1 - 2$) reveals an excess of massive galaxies with respect to predictions of the hierarchical scenario (Cimatti et al. 2004; Glazebrook et al. 2004) or, in other words, that massive ellipticals were already in place at these high redshifts with little subsequent merging, whereas less massive Es present features characteristic of star formation in the more recent past (Ferrerias & Silk 2000). All these observations are contrary to expectations for the hierarchical growth of structure in a cold dark matter-dominated universe, in which large halos form late by coalescence of smaller ones.

These facts lead us to consider models with an “inverted hierarchy” by assuming that less massive galaxies are assembled later than massive ones and, as a consequence, being constituted by a stellar population mix relatively younger than that of bright galaxies. In practice, this means we have abandoned the previous idea in which the starting points for mass assembly and for the beginning of the star formation activity are the same whatever the mass of the galaxy. The departure time for assembly and the beginning of star formation activity was then adjusted in order to improve the location of modeled galaxies in the $H\beta - Mg_2$ diagram.

Moreover, observations suggest that some dust may be mixed with the residual gas in E’s (e.g. Leeuw et al. 2004; Temi, Brighenti & Mathews 2007). A small internal extinction will in particular affect the bluer colors, requiring a slightly higher star formation efficiency to compensate for such a reddening and produce an increase of the $H\beta$ strength. This effect goes in the same sense as down-sizing. Thus, we have included this possibility in our models by assuming that dust is homogeneously mixed with stars. The transfer equation was solved by considering a plane-parallel geometry and, under these conditions, the reddened magnitude in a given filter is given by

$$M_\lambda = M_{\lambda,0} - 2.5 \log \left[\frac{1}{\tau_{eff} (\sqrt{1 - \omega_\lambda} + \coth \tau_{eff})} \right] = M_{\lambda,0} + A_\lambda \quad (5)$$

where $M_{\lambda,0}$ is the unreddened magnitude, ω_λ is the albedo of the dust grains and the effective optical depth τ_{eff} is given by

$$\tau_{eff} = 2 \int \sqrt{1 - \omega_\lambda} \pi a^2 Q_E(\lambda) n_d ds \quad (6)$$

where a is the mean radius of the dust grains, supposed to be spherical, $Q_E(\lambda)$ is the extinction (absorption+scattering) efficiency and n_d is the dust number density. In our calculations, we have assumed that the extinction efficiency and the albedo of the grains have

¹ The required fitting functions for single population synthesis are available under request to the authors

Table 1. Model parameters: columns give respectively the model identification (1), the mass parameter M_0 in units of $10^{11} M_\odot$ (2), the infall time scale in Gyr (3), the wind time scale in Gyr (4), the redshift at which 80% of the mass was assembled (5), the star formation efficiency in Gyr^{-1} (6), the mass fraction lost by the wind (7) and the exponent of the IMF (8)

| Model | M_0 | t_{in} | t_w | z_{80} | k | f_w | γ |
|-------|-------|----------|-------|----------|------|-------|----------|
| 1 | 0.22 | 0.1 | 0.33 | 0.73 | 0.73 | 0.190 | 2.43 |
| 2 | 0.40 | 0.1 | 0.51 | 0.89 | 0.77 | 0.165 | 2.39 |
| 3 | 0.66 | 0.5 | 0.75 | 0.90 | 0.93 | 0.150 | 2.30 |
| 4 | 1.30 | 1.0 | 1.23 | 1.07 | 1.00 | 0.130 | 2.30 |
| 5 | 2.50 | 1.0 | 1.66 | 1.38 | 1.33 | 0.116 | 2.26 |
| 6 | 4.50 | 1.0 | 2.36 | 1.82 | 1.67 | 0.105 | 2.23 |
| 7 | 8.50 | 1.0 | 3.53 | 2.52 | 2.00 | 0.092 | 2.20 |
| 8 | 16.0 | 1.0 | 5.23 | 3.87 | 2.33 | 0.080 | 2.17 |

the same properties as those of galactic dust taken from Cardelli et al. (1989) and Li & Draine (2001) respectively.

3 RESULTS

If previous evolutionary models such as, for instance, those of Kodama & Arimoto (1997) and IMP03 constrained the free parameters by fitting the CMD of ellipticals, these models were unable to adequately reproduce the trend either in the $H\beta - Mg_2$ or in the $Mg_2 - \langle Fe \rangle$ diagrams. The behavior of our best models in these diagrams is illustrated in fig. 1 (middle and lower panels). Indices for the same object measured by different authors, in spite of have being transformed into the Lick system, may differ significantly among them which, besides the intrinsic (cosmic) dispersion, explains the scatter of data points in these diagrams. Even so, the trend of data points in both diagrams is now well reproduced by our model sequence.

Table 1 gives the model parameters found to best describe the mean integrated properties of our galaxies. The first column identifies the model and the second gives the mass parameter M_0 in units of $10^{11} M_\odot$. The actual mass of the galaxy is $M_0(1 - f_w)$, where the mass fraction f_w lost by the galaxy through the wind is given in seventh column. As expected, because of large potential wells, the mass loss fraction decreases for more massive galaxies. The star formation efficiency is given in the sixth column and, as in IMP03, it increases for higher masses. A measure of the down-sizing effect introduced in our models is the redshift z_{80} at which 80% of the mass of the galaxy was already assembled, given in the fifth column. We emphasize again that down-sizing was introduced to improve the location of our models in the $H\beta - Mg_2$ diagram and it is interesting to remark that the required assembling epoch for different masses is not in disagreement with recent observations mentioned above.

Table 2 gives some resulting model properties, including the residual gas fraction, the mean stellar metallicity, and the mean population age.

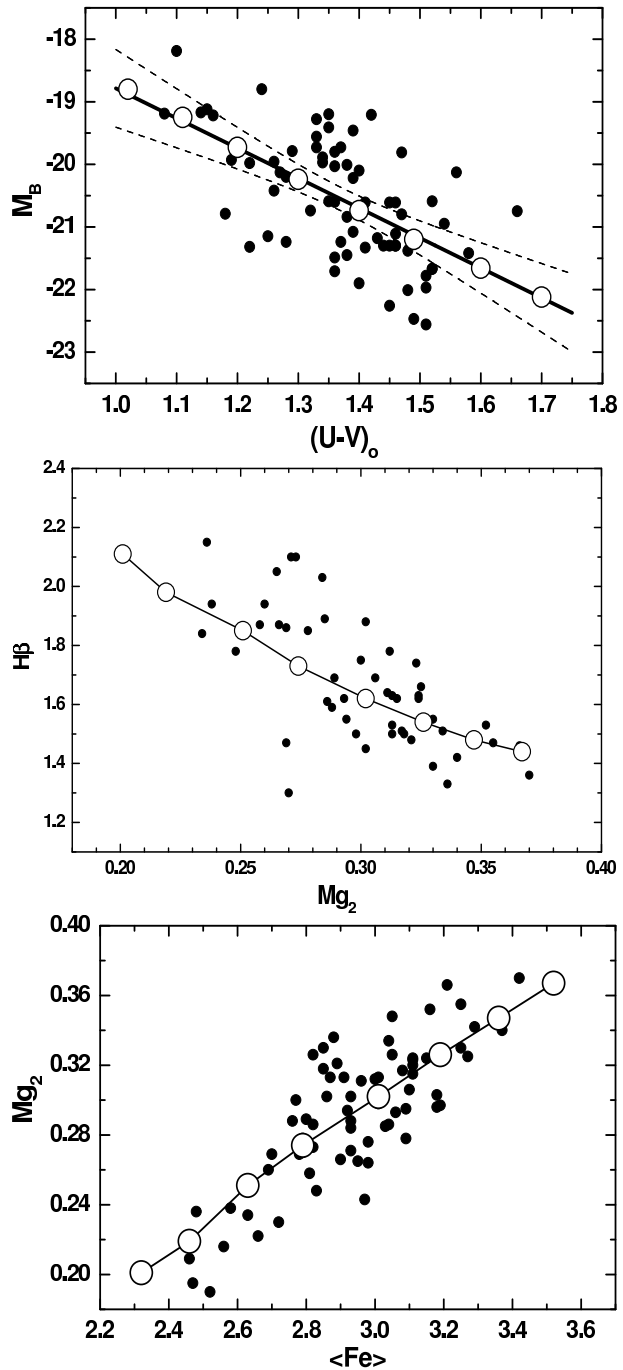


Figure 1. The observed CMD (solid points) is shown in the upper panel, together with the present theoretical results (open circles linked by black segments). The dashed lines indicate the mean dispersion. In the middle and in the lower panels, theoretical metallicity indices (open circles) are compared with data (solid points). Data are from: Worthey et al. (1992), Trager et al. (2000), Mehlert et al. (1998; 2000; 2003), Kuntschner et al. (2001), Proctor et al. (2004) and Howell (2005).

Table 2. Model properties: columns give respectively the model identification (1), the residual gas fraction (2), the fraction of hot gas (3), the mean iron abundance (4), the mean stellar magnesium-to-iron ratio (5), the mean metallicity (6) and the mean population age in Gyr (7)

| Model | f_g | x_h | $[Fe/H]$ | $[Mg/Fe]$ | $[Z/H]$ | age |
|-------|--------|-------|----------|-----------|---------|------|
| 1 | 0.0059 | 0.316 | -0.204 | +0.10 | -0.24 | 6.4 |
| 2 | 0.0062 | 0.369 | -0.139 | +0.15 | -0.16 | 7.2 |
| 3 | 0.0067 | 0.439 | -0.016 | +0.26 | +0.02 | 7.3 |
| 4 | 0.0063 | 0.536 | +0.002 | +0.26 | +0.02 | 8.6 |
| 5 | 0.0056 | 0.685 | +0.082 | +0.32 | +0.12 | 9.7 |
| 6 | 0.0061 | 0.767 | +0.157 | +0.37 | +0.20 | 10.8 |
| 7 | 0.0073 | 0.821 | +0.260 | +0.42 | +0.43 | 11.8 |
| 8 | 0.0089 | 0.862 | +0.437 | +0.50 | +0.47 | 12.8 |

Inspection of table 2 reveals some interesting characteristics of our models. Firstly, the fraction of hot gas increases for more massive galaxies, as X-ray observations indicate, while for galaxies fainter than $M_B \sim -20.0$ most of the residual gas is in the cold phase. For galaxies with absolute magnitudes in the range $-20.3 < M_B < -18.5$, the amount of cold gas (HI) expected from our models is given by the expression

$$\log \frac{M_{HI}}{M_\odot} = -0.677 - 0.455 M_B \quad (7)$$

The HI contents for a sample of E-galaxies in this luminosity range was measured by Lake & Schommer (1984) and are quite consistent with the amount of cold gas predicted by the above relation, differing on the average by $\Delta \log(M_{HI}/M_\odot) \simeq 0.20$. Iron abundances range from \sim half of the solar value for faint objects up to three times solar for the brightest galaxies. The $[Mg/Fe]$ ratio increases with the mass of the galaxy, consequence of an increasing star formation efficiency and a slightly flatter IMF for massive galaxies, with both effects favoring the enrichment of the ISM in α -elements by type II supernovae. Mean population ages now span a wider range (~ 6 Gyr) than obtained in models without down-sizing. Notice that the mean population ages given in table 2 are weighted by mass of alive stars. Had we used a luminosity weighted mean, the resulting values would be reduced approximately by 0.3 Gyr. Larger differences would be expected in the case of IMFs flatter than those characterizing the present models. In order to estimate dust-to-gas mass ratios from the resulting residual gas fraction and the effective extinction, some assumptions are required besides those already mentioned. These concern the average grain radius and its intrinsic density. For this purpose, we have assumed $a = 0.2 \mu\text{m}$ and $\delta = 1.5 \text{ g cm}^{-3}$. Under these conditions, the dust-to-gas ratio varies from ~ 0.003 for the less massive galaxy up to 0.02, for the most massive modeled objects. These values indicate that the relative amount of dust is compatible with the derived metallicities or, in other words, with the amount of metals expected to be in the solid phase.

Tables 3 and 4 give the resulting spectrophotometric properties as colors, the absolute B-magnitude, the stellar mass-to-luminosity ratio, the Lick indices $H\beta$,

Table 3. Photometric properties I: columns give respectively the model identification (1), the absolute B-magnitude (2), the stellar mass-to-luminosity ratio (3), the dust effective extinction (in mag) (4) and the Lick indices $H\beta$, Mg_2 and $\langle Fe \rangle$ respectively in columns (5), (6) and (7)

| Model | M_B | M_*/L_B | A_V | $H\beta$ | Mg_2 | $\langle Fe \rangle$ |
|-------|--------|-----------|-------|----------|--------|----------------------|
| 1 | -18.80 | 3.50 | 0.020 | 2.11 | 0.201 | 2.32 |
| 2 | -19.25 | 4.32 | 0.058 | 1.98 | 0.219 | 2.46 |
| 3 | -19.73 | 4.67 | 0.041 | 1.85 | 0.251 | 2.63 |
| 4 | -20.24 | 5.90 | 0.062 | 1.73 | 0.274 | 2.79 |
| 5 | -20.74 | 7.25 | 0.062 | 1.62 | 0.302 | 3.01 |
| 6 | -21.20 | 8.64 | 0.080 | 1.54 | 0.326 | 3.19 |
| 7 | -21.66 | 10.85 | 0.150 | 1.48 | 0.347 | 3.36 |
| 8 | -22.12 | 13.54 | 0.201 | 1.44 | 0.367 | 3.52 |

Table 4. Photometric properties II: columns give respectively the model identification (1) and the integrated colors

| Model | (U-V) | (B-V) | (V-R) | (V-I) | (V-K) |
|-------|-------|-------|-------|-------|-------|
| 1 | 1.02 | 0.798 | 0.518 | 1.049 | 2.566 |
| 2 | 1.11 | 0.838 | 0.538 | 1.085 | 2.643 |
| 3 | 1.20 | 0.870 | 0.544 | 1.094 | 2.678 |
| 4 | 1.30 | 0.908 | 0.563 | 1.129 | 2.744 |
| 5 | 1.40 | 0.941 | 0.580 | 1.157 | 2.815 |
| 6 | 1.49 | 0.977 | 0.595 | 1.189 | 2.892 |
| 7 | 1.60 | 1.026 | 0.622 | 1.244 | 3.015 |
| 8 | 1.70 | 1.058 | 0.644 | 1.290 | 3.116 |

Mg_2 , $\langle Fe \rangle$ and the dust effective extinction (in mag) in the V band.

Using the derived properties of our models, we have derived relations between the mean age of stellar population mix and observed integrated properties such as the indices $H\beta$, $\langle Fe \rangle$ and the color (U-V). These are

$$\tau_1 = -19.230 + 3.884H\beta + 7.516 \langle Fe \rangle \quad (8)$$

$$\tau_2 = 3.122 - 3.243(U - V) + 1.226 \langle Fe \rangle^2 \quad (9)$$

where ages are in Gyr. The mean iron abundance and the mean magnesium-to-iron ratio of the stellar population mix can be estimated from the relations

$$[Fe/H] = -1.694 - 3.220Mg_2 + 0.963 \langle Fe \rangle \quad (10)$$

and

$$[Mg/Fe] = -0.674 + 0.363 \langle Fe \rangle - 0.318Mg_2 \quad (11)$$

Once the mean iron abundance and the mean magnesium-to-iron ratio are calculated from the relations above, the mean metallicity can be derived from

$$[Z/H] = -0.313 + 0.399[Fe/H] + 1.242[Mg/Fe] \quad (12)$$

The scatter of data observed in figure 1 is due essentially to measurement errors and to intrinsic variations of physical parameters among galaxies of same mass. We have estimated the dispersion of data with respect to our models, correcting for measurement errors. Then, from simple error propagation, we have estimated the uncertainties in the calibrations above. These correspond to about 1.5 and 1.0 Gyr for ages estimated from eqs. 8

and 9 respectively, 0.17dex for metallicities and 0.1dex for the $[Mg/Fe]$ ratio. Systematic errors may certainly increase these estimates.

In order to perform an application of the present models and compare with the results derived by using the SSP approach, we have selected 42 galaxies whose ages and metallicities were estimated by Howell (2005). For some of these galaxies, Thomas et al. (2005) have also derived ages and metallicities, which will also be used in our comparative analysis. Mean population ages and mean metallicities derived from our calibrations are given in table 5. Ages are the average value resulting from the aforementioned calibrations and are followed by an index a or b . The former implies that the average age value differs by less than 1 Gyr from the individual determinations whereas the later means that the difference is in the range 1-2 Gyr. Age differences in this range implies that data points are not close to the mean theoretical relations and, consequently, the resulting age or metallicity values are more uncertain.

It is important to mention that ages derived from SSP models either by Howell (2005) or by Thomas et al. (2005) are consistent but with values given by the latter authors being systematically higher by ~ 1.5 Gyr than those by the former author. The same remark is valid for metallicities, excepting that for $[M/H] > 0.5$ the values derived by Howell are higher than those by Thomas et al. In fig. 2 (upper panel) we have plotted metallicities as a function of ages derived from SSP, using the results by Howell and including those by Thomas et al. for the same objects. In spite of the significant scatter, we notice that "young" objects, with ages < 5 Gyr are those with the highest metallicity while galaxies with lower metallicities are generally old. This behavior is completely different when a similar plot is performed with values obtained from our evolutionary models (fig. 2, lower panel). In this case, a robust correlation between the mean metallicity and the mean population age is observed, indicating that the most massive galaxies are those which have been more enriched in chemical elements thanks to the higher star formation efficiency. The most discrepant object in this plot is NGC 3610, for which the mean population age determination gives values discrepant by ~ 2.5 Gyr, indicating that the model parameters which characterize this galaxy are far from those describing the mean trend. This galaxy is likely to be a merger remnant, and merits more detailed structural modeling (cf. Strader, Brodie and Forbes 2004), beyond the scope of this paper. However, if an important merger event stimulates the star formation activity, this can roughly be simulated in our approach by a higher star formation efficiency. In fact, with $k = 3.96 \text{ Gyr}^{-1}$ (instead of 1.33 Gyr^{-1} for a galaxy of same luminosity) it is possible to reproduce quite well the observed colors and Lick indices of NGC 3610. In this case, the mean population age would be 2.8 Gyrs , indicative of the epoch of the merger episode. Notice also that, in general, our derived ages span the interval 7-12 Gyr while for the same galaxies, the resulting interval from the SSP approach is 2.3-19 Gyr.

It is worth mentioning a further aspect when comparing results derived from SSP models and EVM. The

Table 5. Ages & Metallicities: column (1) identifies the galaxy; column (2) gives the mean population age in Gyr; the label (a) means that the average between the two calibrations differs by less than 1 Gyr from individual age determinations while (b) means that the difference is in the range 1-2 Gyr; columns (3) and (4) give the mean magnesium-to-iron ratio and the mean metallicity, both with respect to solar values, while the next two columns, for comparison, give ages and metallicities derived from SSP by Howell (2005).

| NGC | age | $[Mg/Fe]$ | $[Z/H]$ | age_H | $[Z/H]_H$ |
|------|----------|-----------|---------|---------|-----------|
| 0315 | 10.7 (a) | +0.35 | +0.23 | 5.0 | +0.44 |
| 0584 | 11.3 (a) | +0.35 | +0.26 | 2.4 | +0.61 |
| 0596 | 8.2 (a) | +0.22 | +0.26 | 4.4 | +0.22 |
| 0636 | 10.5 (a) | +0.33 | +0.23 | 3.8 | +0.44 |
| 1052 | 8.3 (a) | +0.27 | +0.03 | 16.0 | +0.42 |
| 1172 | 7.8 (a) | +0.18 | -0.07 | 4.8 | +0.13 |
| 1209 | 9.3 (a) | +0.33 | +0.17 | 15.6 | +0.28 |
| 1400 | 8.1 (a) | +0.26 | +0.02 | 14.2 | +0.31 |
| 1700 | 12.0 (a) | +0.38 | +0.33 | 2.3 | +0.63 |
| 2300 | 10.3 (a) | +0.36 | +0.22 | 5.5 | +0.48 |
| 2768 | 8.2 (a) | +0.28 | +0.18 | 10.0 | +0.14 |
| 2778 | 8.8 (a) | +0.29 | +0.12 | 5.0 | +0.40 |
| 3115 | 11.7 (a) | +0.41 | +0.36 | 3.9 | +0.65 |
| 3193 | 8.3 (a) | +0.26 | +0.02 | 11.8 | +0.20 |
| 3377 | 7.8 (a) | +0.20 | -0.02 | 3.5 | +0.30 |
| 3379 | 10.3 (a) | +0.35 | +0.23 | 8.0 | +0.32 |
| 3607 | 8.6 (a) | +0.27 | +0.05 | 10.6 | +0.27 |
| 3608 | 7.9 (a) | +0.23 | +0.00 | 6.1 | +0.38 |
| 3610 | 10.8 (b) | +0.31 | +0.00 | 1.7 | +0.76 |
| 3640 | 9.4 (a) | +0.29 | +0.15 | 4.9 | +0.26 |
| 4168 | 8.9 (a) | +0.26 | +0.09 | 5.0 | +0.24 |
| 4365 | 11.3 (a) | +0.40 | +0.36 | 5.9 | +0.59 |
| 4374 | 10.0 (a) | +0.34 | +0.22 | 11.1 | +0.24 |
| 4472 | 11.9 (a) | +0.44 | +0.42 | 7.8 | +0.36 |
| 4473 | 10.5 (a) | +0.35 | +0.24 | 4.0 | +0.46 |
| 4486 | 8.8 (b) | +0.32 | +0.14 | 19.6 | +0.27 |
| 4489 | 9.1 (a) | +0.22 | +0.14 | 2.3 | +0.24 |
| 4552 | 11.1 (a) | +0.39 | +0.29 | 10.5 | +0.32 |
| 4621 | 10.5 (a) | +0.36 | +0.22 | 15.8 | +0.29 |
| 4697 | 8.4 (a) | +0.23 | -0.02 | 7.1 | +0.19 |
| 5576 | 10.2 (a) | +0.30 | +0.17 | 2.5 | +0.60 |
| 5638 | 8.6 (a) | +0.27 | +0.05 | 7.8 | +0.32 |
| 5813 | 9.3 (a) | +0.30 | +0.12 | 14.9 | +0.07 |
| 5831 | 7.6 (a) | +0.25 | +0.04 | 2.7 | +0.61 |
| 5846 | 8.3 (a) | +0.27 | +0.06 | 12.2 | +0.25 |
| 6702 | 9.2 (b) | +0.24 | +0.07 | 1.4 | +0.80 |
| 6703 | 9.6 (a) | +0.29 | +0.11 | 3.9 | +0.39 |
| 7454 | 7.3 (a) | +0.15 | -0.15 | 4.7 | +0.04 |
| 7562 | 10.2 (a) | +0.35 | +0.25 | 7.1 | +0.31 |
| 7619 | 12.2 (a) | +0.45 | +0.41 | 13.5 | +0.31 |
| 7626 | 10.7 (a) | +0.37 | +0.24 | 12.0 | +0.27 |
| 7785 | 10.6 (a) | +0.36 | +0.26 | 7.9 | +0.31 |

present sequence of models was built by varying different parameters in order to adequately reproduce the integrated properties such as luminosities, colors and metallicity indices. In this sense, the present models are "self-consistent". In general, analyses based on SSP models use only metallicity indices but not colors. If ages and metallicities derived from SSP models are used to predict the colors of the object, we obtain values considerably redder in comparison with observations. The reason for this behavior is that all stars in SSP models

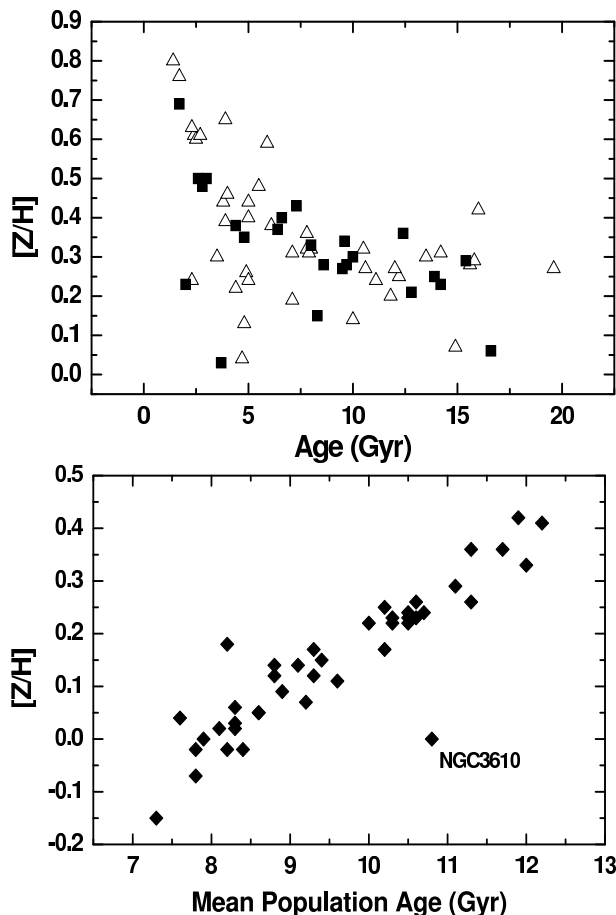


Figure 2. Upper panel: metallicities as a function of ages derived from SSP models. Open triangles are Howell (2005) data while solid squares are Thomas et al. (2005) data for common galaxies listed in table 4. Lower panel: the same plot but for ages and metallicities derived from the present model.

have the same metallicity while in evolutionary models, stars of low-metallicity are also present in the population mix, contributing to the total light and producing bluer colors. This effect is illustrated in fig. 3 in which, for galaxies listed in table 5, the predicted $(U-V)$ colors derived from SSP metallicities and ages are plotted against observed values.

4 CONCLUSIONS

In this study, new models for E-galaxies are presented. The “canonical” one-zone model was revised by including a simplified two-phase interstellar medium, in which stars are formed only in cold regions and a galactic wind removes hot gas from the galaxy. The mass of the galaxy increases with time as a consequence of infall, here represented by either continuous accretion or discrete minor merger events. The possibility that some dust is mixed with the residual gas was also taken into account. The different parameters of the model were varied in order to adequately reproduce integrated properties such

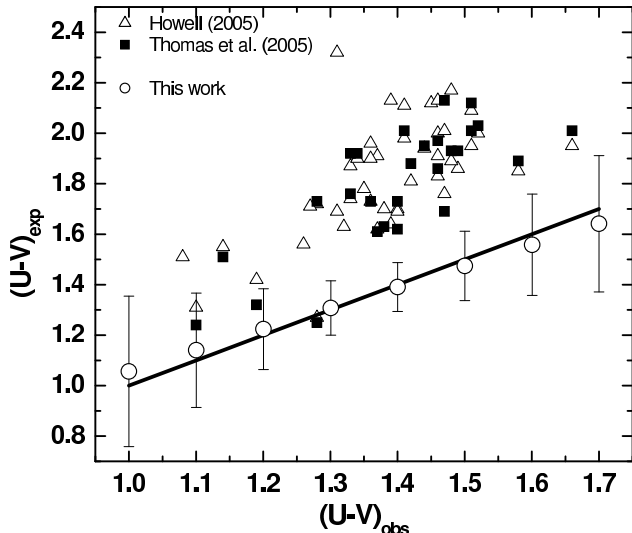


Figure 3. Predicted versus observed $(U-V)$ colors. The open triangles and solid squares identify the source for SSP ages and metallicities. The solid line represents the expected correspondence. Open circles represents predictions of our models. Observed colors were averaged within bins of magnitude ΔM_B . The corresponding dispersions are also indicated.

as the color-magnitude diagram and the trends of indices such as $H\beta$ vs. Mg_2 and Mg_2 vs. $\langle Fe \rangle$.

The fundamental characteristic of these models concerns the beginning of stellar assembly and star formation activity. The start-up time was adjusted in order to give a better description of data in the $H\beta$ - Mg_2 diagram and this requires that the less massive galaxies are assembled later, in agreement with the down-sizing effect. In order to characterize this effect, we have defined the quantity z_{80} , corresponding to the redshift at which 80% of the (baryonic) mass was assembled. Galaxies in the luminosity range $-18.8 > M_B > -20.2$ were assembled in the redshift range $0.7 < z_{80} < 1.1$ whereas brighter objects $-21.2 > M_B > -22.2$ were assembled earlier, e.g., $1.8 < z_{80} < 3.9$.

Our models predict an increasing fraction of hot gas for massive galaxies, a consequence of gravitational trapping, in concordance with X-ray observations. The derived amount of dust mixed with the residual gas also increases with galaxian masses and the dust-to-gas ratio varies from 0.003 for faint up to 0.02 for bright galaxies. However, these numbers depend on the adopted grain dimension and composition. Thanks to down-sizing, the resulting mean stellar population ages span a range of 6.4-12.8 Gyr, considerably wider than our previous models (IMP03). Metallicities vary from half to about three times solar, increasing with the mass of the galaxy. These results imply that the CMD is not either a pure metallicity or a pure age sequence, but a combination of these two quantities.

From the present models, different calibrations were obtained allowing estimates of mean properties of the stellar population mix like the age, the metallicity and the $[Mg/Fe]$ ratio, from the knowledge of integrated parameters like the $(U-V)$ color and the Lick indices $H\beta$, Mg_2 and $\langle Fe \rangle$. These calibrations were applied

to a sample of early type galaxies, whose spectral indices were interpreted in terms of SSP models. From these studies based on SSP models, galaxies with stellar population ages as young as 2.5 Gyr can be found, while the corresponding ages derived from our model calibrations are significantly higher, ranging from 7.5 up to 12 Gyr.

The mean values for metallicities and ages concern the bulk of the stellar population mix constituting ellipticals. However, the residual gas originated either from the stellar evolution or infall can presently be converted into stars. In fact, Ferreras & Silk (2000) studied a sample of early type galaxies in Abell 851 and found that the slope and scatter in the near-ultraviolet (NUV)-optical plane are consistent with some objects having $\sim 10\%$ of their stellar mass in stars younger than ~ 0.5 Gyr. The study of a large sample by Kaviraj et al. (2006) confirms such a conclusion. They have noticed that about 30% of the galaxies in their sample (~ 2100 objects) have UV-optical colors consistent with some star formation activity within the last Gyr. This recent activity represents, according to their estimates, about 1-3 % of the stellar mass in stars less than 1 Gyr old. Using the fraction of residual cold gas and the star formation efficiency of our models, we have estimated the mass fraction of stars formed in the last 0.8 Gyr, which are in the range 2.3-5.7 %, fully consistent with UV and NUV observations.

As mentioned, the present models describe mean integrated properties and some uncertainties are certainly present in the resulting calibrations of age and metallicity, because of cosmic scatter and observational errors. In a future paper we will report the application of the present model to individual galaxies, deriving the relevant parameters from the best fit of the integrated parameters of each object. This approach will possibly give information about the cosmic scatter and will eventually reveal any possible correlations with the environment.

Acknowledgments T.P. Idiart thanks to FAPESP (grant 2006/01025-3) for the financial support during the stay at Oxford.

REFERENCES

Baugh, C. M., Cole, S., Frenk, C. S., 1996, MNRAS, 283, 1361
 Baugh, C. M., Cole, S., Frenk, C. S., Lacey, C. G., 1998, ApJ, 498,504
 Borges, A. C., Idiart, T. P., de Freitas Pacheco, J. A., Thevenin, F., 1995, AJ, 110, 2408
 Bressan, A., Chiosi, C., Tantalo, R., 1996, A&A, 311, 425
 Cardelli, J.A., Clayton, G.C., Mathis, J.S., 1989, ApJ, 345, 245
 Chiosi, C., Carraro, G., 2002, MNRAS, 335, 335
 Cimatti, A. et al., 2004, Nature 430, 184
 Cowie, L.L., Songaila, A., Hu, E.M., Cohen, J.G., 1996, AJ 112, 839
 de Freitas Pacheco, J.A., Michard, R. & Mohayaee, R., 2003 in Recent Res. Devel. Astron.& Astrophys. 1, 271 (arXiv:astro-ph/0301248)

Faber, S.M., Worthey, G. and Gonzalez, J.J., 1992, in IAU Symp. 149 - The Stellar Populations of Galaxies - eds. B.Barbuy and A. Renzini, Kluwer Academic Publishers, p.255
 Ferreras, I., Silk J., 2000, ApJ, 541, L37
 Ferrini, F., Poggianti, B. M., 1993, ApJ, 410, 44
 Fujita, Y., Fukumoto, J., Okoshi, K., 1996, ApJ, 470, 762
 Fujita, Y., Fukumoto, J., Okoshi, K., 1997, ApJ, 488, 585
 Gibson, B.K., 1997, MNRAS, 290, 471
 Girardi, L., Bressan, A., Bertelli, G., Chiosi, C., 2000, A&AS, 141, 371
 Glazebrook, K. et al., 2004, Nature, 430, 181
 Howell, J.H., 2005, AJ, 130, 2065
 Idiart, T. P., de Freitas Pacheco, J. A. 1995, AJ, 109, 2218
 Idiart, T. P., de Freitas Pacheco, J. A., Costa, R. D. D., 1996, AJ, 111, 1169
 Idiart, T.P., Michard, R., de Freitas Pacheco, J.A., 2003, A&A, 398, 949
 Juneau, S. et al., 2005, ApJ, 619, 135
 Kauffmann, G., 1996, MNRAS, 281, 87
 Kaviraj, S., Devriendt, J.E.G., Ferreras, I., Yi, S.K., 2005, MNRAS, 360, 60
 Kaviraj, S., et al., 2006, ApJS accepted, (arXiv:astro-ph/0601029)
 Kim, Y-C., Demarque, P., Yi, S.K., Alexander, D.R., 2002, ApJS, 143, 499
 Kodama, T., Arimoto N., 1997, A&A, 320, 41
 Kuntschner, H., Lucey, J. R., Smith, R. J., Hudson, M. J., Davies, R. L., 2001, MNRAS, 323, 615
 Lake, G., Schommer, R.A., 1984, ApJ 280, 107
 Larson, R.B., 1974a, MNRAS, 166, 585
 Larson, R.B., 1974b, MNRAS, 169, 229
 Leeuw, L.L., Sansom, A.E., Robson, E.I., Haas, M., Kuno, N., 2004, ApJ, 612, 837
 Li, A., Draine, B.T., 2001, ApJ, 554, 778
 Lotz, J. M., Ferguson, H. C., Bohlin, R. C., 2000, ApJ, 532,830
 Matteucci, F., Tornambe, A., 1987, A&A, 185, 51
 Matteucci, F., 2003, Ap&SS, 284, 539
 Mehlert, D., Saglia, R., Bender, R., Wegner, G., 1998, A&A, 332, 33
 Mehlert, D., Saglia, R. P., Bender, R., Wegner, G., 2000, A&AS, 141, 449
 Mehlert, D., Thomas, D., Saglia, R. P., Bender, R., Wegner, G., 2003, A&A, 407, 423
 Miranda, O., 1992, thesis, Universidade de S.Paulo
 Nomoto, K., Hashimoto, M., Tsujimoto, T., Thielemann, F. -K., Kishimoto, N., Kubo, Y., Nakasato, N., 1997a, Nuclear Physics A 616, 79c
 Nomoto, K., Iwamoto, K., Nakasato, N., Thielemann, F. -K., Brachwitz, F., Tsujimoto, T., Kubo, Y., Kishimoto, N., 1997b, Nuclear Physics A 621, 467c
 Peebles, P. J. E., 2002, ASP Conf. Ser. Vol. 283, A New Era in Cosmology. Astron. Soc. Pac., San Francisco, p. 351
 Proctor, R. N., Forbes, D. A., Hau, G. K. T., Beasley, M. A., De Silva, G. M., Contreras, R., Terlevich A. I., 2004, MNRAS, 349, 1381
 Sadler, E. M. 1992, in IAU Symp. 149, The Stellar Populations of Galaxies, ed. B. Barbuy & A. Renzini (Dordrecht: Kluwer), p.41
 Salaris, M., Chieffi, A., Straniero, O., 1993, ApJ, 414, 580
 Salasnich, B., Girardi, L., Weiss, A., Chiosi, C., 2000, A&A, 361, 1023
 Schweizer, F., Seitzer, P. 1992, AJ, 104, 1039
 Silk J. 2004, in "Where Cosmology and Fundamental Physics Meet, 23-26 June, Marseille, France" (arXiv:astro-ph/0401032)
 Scodreggio, M., 2001, AJ, 121, 2413

- Strader, J., Brodie, J. and Forbes, D. 2004, *AJ*, 127, 295
- Tantalo, R., Chiosi, C., Bressan, A., 1998, *A&A*, 333, 419
- Tem, P., Brighenti, F., Mathews, W. 2007, *ApJ* in press
(arXiv:astro-ph/0701431)
- Thielemann, F-K, Nomoto, K., Hashimoto, M., 1996, *ApJ*,
460, 408
- Thomas, D., Maraston C., Bender R., 2003, *MNRAS*, 339,
897
- Thomas, D., Maraston, C., Bender, R., Mendes de Oliveira,
C., 2005, *ApJ*, 621, 673
- Toomre, A., 1977, in Tinsley B. M., Larson T. B., eds, *Evolution
of Galaxies and Stellar Populations*. Yale University
Observatory, New Haven, CT, p. 401
- Trager, S. C., Faber, S. M., Worthey, G., Gonzalez, J.J., 2000,
AJ, 119, 1645
- Vazdekis, A., Caruso, E., Peletier, R.F., Beckman, J.E., 1996,
ApJS, 106, 307
- White, S.D.M., Rees, M.J., 1978, *MNRAS* 183, 341
- Worthey, G. et al., 1992, *ApJ* 398, 69
- Worthey G., 1994, *ApJS*, 95, 107
- Worthey, G., 1998, *PASP*, 110, 888